This is an open access article published under an ACS AuthorChoice License, which permits copying and redistribution of the article or any adaptations for non-commercial purposes.

Environmental Science & Technology

Article

pubs.acs.org/est

Coupled Effects of Aging and Weak Magnetic Fields on Sequestration of Selenite by Zero-Valent Iron

Liping Liang,[†] Xiaohong Guan,*[,†] Zhong Shi,[∥] Jialing Li,[‡] Yinan Wu,[‡] and Paul G. Tratnyek*[,§]

[†]State Key Lab of Urban Water Resource and Environment, Harbin Institute of Technology, Harbin 150090, Heilongjiang, PR China

[‡]State Key Laboratory of Pollution Control and Resources Reuse, College of Environmental Science and Engineering, Tongji University, Shanghai 200092, PR China

[∥]The Department of Physics, Tongji University, Shanghai 200092, PR China

[§]Institute of Environmental Health, Oregon Health & Science University, 3181 SW Sam Jackson Park Road, Portland, Oregon 97239-3098, United States

Supporting Information

ABSTRACT: The sequestration of Se(IV) by zero-valent iron (ZVI) is strongly influenced by the coupled effects of aging ZVI and the presence of a weak magnetic field (WMF). ZVI aged at pH 6.0 with MES as buffer between 6 and 60 h gave nearly constant rates of Se(IV) removal with WMF but with rate constants that are 10- to 100-fold greater than without. XANES analysis showed that applying WMF changes the mechanism of Se(IV) removal by ZVI aged for 6−60 h from adsorption followed by reduction to direct reduction. The strong correlation between Se(IV) removal and Fe^{2+} release suggests direct reduction of Se(IV) to Se(0) by Fe^0, in agreement with the XANES analysis. The numerical simulation of ZVI magnetization revealed that the WMF influence on Se(IV) sequestration is associated mainly with the ferromagnetism of ZVI and the paramagnetism of Fe^{2+}. In the presence of the WMF, the Lorentz force gives rise to convection in the solution, which narrows the diffusion layer, and the field gradient force, which tends to move paramagnetic ions (esp. Fe^{2+}) along the higher field gradient at the ZVI particle surface, thereby inducing nonuniform depassivation and eventually localized corrosion of the ZVI surface.

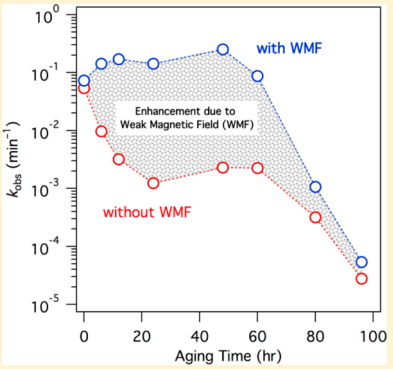

INTRODUCTION

Zero-valent iron (ZVI) has been shown to remove a wide variety of contaminants from water by a mixture of transformation, adsorption, and coprecipitation processes. The relative significance of these processes varies with the type of contaminant, condition of the ZVI, solution chemistry, and hydrodynamic operating conditions. In cases where contaminants are not degraded, but rather are removed by transfer from the aqueous to solid phase, the overall treatment process is referred to as cementation[1] or sequestration.[2,3] Sequestration by ZVI is applicable to almost all heavy metals[4,5] and has been studied intensively for some, especially the oxyanion-forming metals chromium,[6−8] arsenic,[9−11] and uranium.[12−14]

The sequestration of metals in ZVI-based systems is generally favored by the growth and accumulation of iron oxides—and other iron-containing solid phases—that are formed by the Fe^{2+} released during corrosion of Fe^0.[15] However, the specific effects of these authigenic phases are multiple and variable, so the relative importance of specific effects is not always clear, despite many studies that have addressed aspects of this issue. For example, although thicker passive films (and the formation of secondary authigenic phases) increase the surface area for contaminant removal by nonreductive processes, breakdown of the passive film on ZVI generally favors contaminant reduction by exposing more strongly reducing surface area.[16,17] When ZVI is deployed for water treatment under oxic conditions, the role of authigenic iron oxides is even more critical because the phase transformations are more dynamic and oxidative pathways for contaminant treatment become more significant.[18]

There are many factors that determine the structure and composition of the oxide phases associated with ZVI under remediation conditions, the most widely recognized and thoroughly studied being solution chemistry. For example, it has long been known that nitrate in the medium passivates ZVI, resulting in slower reduction of cocontaminants[19−21] and that dissolved carbonate is corrosive in the short term but passivating in the long run, resulting in a parallel dependence of cocontaminant reduction rates.[22−24] Recent studies have documented analogous effects for other medium components, including additional inorganic anions,[9,20] various cations,[25−27] and polyelectrolytes.[28−30] In most cases, changes in medium composition induce changes in the oxide film that take place

Received: February 25, 2014
Revised: May 2, 2014
Accepted: May 7, 2014
Published: May 7, 2014

 © 2014 American Chemical Society

over time frames of hours to days or weeks, resulting in transformations that are collectively referred to as "aging". Aging effects are relevant to laboratory- and field-scale applications of ZVI for water treatment, so the increased attention to them in recent studies (e.g. refs 31−34) is an important development in the maturation of this field.

Given the key role that oxide/passive films play in the—short- and long-term—performance of ZVI in remediation applications, it is inevitable that many strategies for maintaining or enhancing ZVI treatments involve manipulating the properties of the oxides. The earliest example of this was acid washing, which removes oxides and therefore increases the rates of contaminant reduction in laboratory tests.[35−38] Another example is ultrasonication, which favors contaminant degradation by physically disrupting the oxide coating on ZVI and may also dislodge oxide precipitates that obstruct pore channels in reactive barriers.[39−42] A third approach involves application of an electrical potential from an external source to reduce the oxides that comprise the passive film, thereby increasing reaction rates and possibility adding to the longevity of ZVI treatments.[43,44] Recently, we reported evidence in support of another approach to enhancing ZVI performance: application of a weak magnetic field (WMF), which can accelerate corrosion of ZVI resulting in greater dissolution of Fe^{2+} and more rapid sequestration of Se(IV).[45]

The evidence for a WMF effect on contaminant removal by ZVI presented in our previous work[45] was limited to Se(IV) sequestration by one high-purity micrometer-sized ZVI in media representing two solution chemistry variables (pH varied from 4 to 7.2, initial Se(IV) concentration varied from 5 to 40 mg L^{-1}). This leaves a wide range of factors to be considered before the overall—fundamental and/or practical—significance of the WMF effect can be assessed. Since the WMF effect likely arises from changes in the oxides associated with ZVI, operational factors that determine oxide film conditions are the highest priority. Therefore, in this study, we investigated the effect of aging ZVI on the WMF effect in a series of controlled batch experiments designed to demonstrate how the two effects are coupled. To accomplish this, we (*i*) prepared aged ZVI (AZVI) for time periods from 0 to 96 h and characterized the structure and composition of the resulting materials, (*ii*) measured and compared the Se(IV) sequestration kinetics using pristine (unaged) and AZVI; and (*iii*) numerically simulated the distribution of magnetic flux density and the magnetic field gradient around ZVI particles after exposure to a WMF. Future work will address the WMF effect in delaying ZVI passivation and recovering the reactivity of passivated ZVI from permeable reactive barrier under conditions of reactive-transport.

MATERIALS AND METHODS

Materials. All chemicals were of analytical grade and used as received. The ZVI described in our previous study was also used in this study.[45] This material is high purity Fe^0 (99.8−99.9%) with mean diameter (D_{50}) ∼7.4 μm and BET specific surface area (a_s) = 0.3015 m^2/g. All the other chemicals were purchased from Shanghai Qiangshun Chemical Reagent Company. The stock solutions were prepared by dissolving the corresponding salts in ultrapure water generated from a Milli-Q Reference water purification system.

Synthesis and Characterization of AZVI. To synthesize the AZVI samples, 10.0 g of pristine ZVI particles was incubated in 0.5 L of doubly distilled water buffered at pH 6.0 ± 0.1 with 0.20 M 2-(*N*-morpholino)ethanesulfonic acid (MES) for different exposure times. MES was chosen for this work for the same reason that it was used in so many other studies with ZVI.[35] Aging was performed in wild-mouth bottles open to the air with mixing at 310 rpm using a propeller type stirrer (D2004W, Shanghai Sile Instrument Co., Ltd.). The suspension pH was monitored frequently and, if necessary, was readjusted to pH 6.0 ± 0.1 with NaOH or HCl. Eight kinds of AZVI were synthesized by aging the pristine ZVI in MES buffer for 0, 6, 12, 24, 48, 60, 80, and 96 h, which were denoted as AZVI-0, AZVI-6, AZVI-12, AZVI-24, AZVI-48, AZVI-60, AZVI-80, and AZVI-96, respectively. The precipitates were collected after predetermined intervals, washed with DI water, freeze-dried, and then kept in a glovebox for subsequent characterization and use. The prepared AZVI samples were subject to Field Emission Scanning Electron Microscopy (FE-SEM), XRD, Raman, and BET analysis, and the details were present in Text S1 in Supporting Information.

Batch Experiments and Chemical Analysis. To investigate the feasibility of depassivating AZVI with WMF, the experimental setup employed in our previous study[45] was also used here. In brief, two cylindrical neodymium−iron−boron permanent magnets with a diameter of 30 mm and a height of 5 mm on an iron sheet were placed under the reactor, which provided a maximum magnetic field intensity of ∼20 mT at the bottom of the reactor throughout the course of the experiment. Each batch reactor received 0.50 g of ZVI and 0.5 L of aqueous medium (i.e., 1.0 g L^{-1} ZVI). The aqueous medium consisted of 40.0 mg L^{-1} Se(IV), 0.01 M NaCl, and 0.1 M MES as buffer. All experiments were carried out open to the air, and the solution was mixed at 310 rpm at 25 °C. At this stirring intensity, the ZVI was uniformly suspended, and aggregation was not observed. The oxidation−reduction potential (ORP) of this suspension was monitored in situ with an Pt ORP sensor connected to a pHS-3C pH meter, and the concentration of dissolved oxygen (DO) was determined in situ with a JPB-607 portable DO analyzer (Shanghai Precision & Scientific Instrument Co Ltd.). All experiments were run in duplicate or triplicate, and the replicates were averaged for use in figures and fitting. The corresponding standard deviations, or standard errors, are shown where appropriate.

At fixed time intervals, 5 mL of suspension was taken, filtered through a 0.22 μm pore size membrane, acidified with one drop of 65% HNO_3, and analyzed for selenium concentration using a PerkinElmer Optima 5300 DV ICP-OES. Fe^{2+} concentration was examined with the modified ferrozine method using a TU-1901 UV/visible spectrophotometer at the wavelength of 562 nm following the procedure of Stookey.[46] In order to investigate the valence of Se in the precipitates, the reacted ZVI samples were collected at different intervals, washed with distilled water, freeze-dried, and put into zippered bags before subjecting to Se *K*-edge X-ray Absorption Near Edge Structure (XANES) analysis. The details of XANES analysis were present in Text S1 in the Supporting Information.

Magnetic Field Characterization. The strength, direction, and gradient of magnetic field induced by ZVI particles was characterized using 3D magnetic field numerical simulation software (Amperes and Magneto, from Integrated Engineering Software Inc.), assuming that a 10 μm diameter pure Fe^0 sphere was exposed to an external homogeneous magnetic field with flux density of 10 mT. Experimental visualization of the WMF effect on Fe^0 corrosion was performed with iron wire, as describe in Text S2 in the Supporting Information.

dx.doi.org/10.1021/es500958b | Environ. Sci. Technol. 2014, 48, 6326−6334

RESULTS AND DISCUSSION

Material Characterization. Characterization of the ZVI used in this study by XRD (Figure S1) confirmed that the major component of the pristine material (AZVI-0) was α-Fe^0 (JCPDS 06-0696). XRD peaks corresponding to magnetite (Fe_3O_4, JCPDS 88-0315) started to appear at 12 h (AZVI-12) and then increased in intensity progressively with further aging. Peak intensity for Fe^0 decreased with aging, disappearing completely in AZVI-96 with concomitant appearance of two new peaks identified to be lepidocrocite (γ-FeOOH, JCPDS 74-1877). The data in Figure S1 were used to estimate Fe^0 and Fe_3O_4 content during aging, and the results are shown in Figures 1A and B. The Fe^0 content decreases linearly with aging

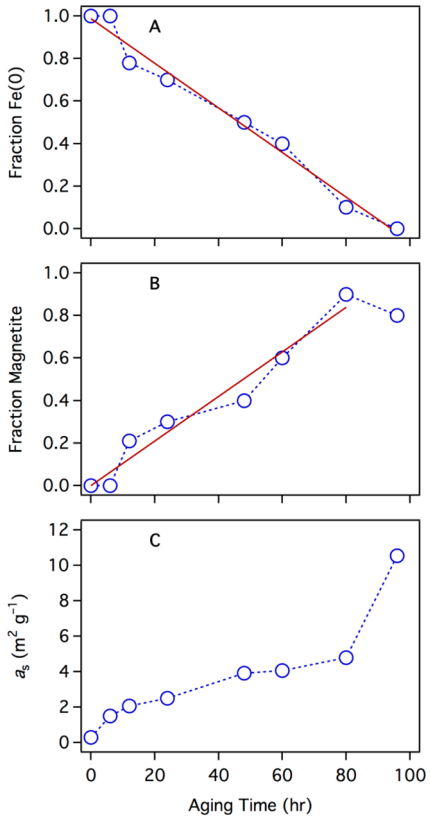

Figure 1. Effects of aging on three material properties of ZVI: (**A**) Fraction Fe^0 from XRD, (**B**) Fraction magnetite from XRD, and (**C**) Specific surface area (a_s) from BET gas adsorption. Regression lines are (A) $y = 0.99 \pm 0.03 + -0.0105 \pm 0.0006x$ with $r^2 = 0.98$ and (B) $y = -0.0004 \pm 0.04 + 0.010 \pm 0.001x$ with $r^2 = 0.95$.

time, with a slope of 0.010 ± 0.001 fraction Fe^0 h^{-1}. The increase in Fe_3O_4 is linear up to 80 h—with a slope that matches that for the Fe^0 fraction—although the Fe_3O_4 content decreases in the AZVI-96 sample, presumably due to further oxidation to γ-FeOOH. The rate and extent of ZVI oxidation represented by the data in Figures 1A and B corresponds to aging in a stirred and open system, so it is much faster than the aging kinetics reported in previous studies that were done under anoxic conditions.[34,47]

The Raman spectra for the samples of aged ZVI are shown in Figure S2. In all of the samples, magnetite is indicated by the Raman bands at 215, 276, 395, 584, and 1280 cm^{-1}.[48] The size of these bands appears to increase with aging time, which is consistent with results obtained by XRD. A peak at 486 cm^{-1}, which may be due to lepidocrocite,[49] is barely evident in the Raman spectrum for AZVI-6 but grows substantially over the aging period. The earlier detection of γ-FeOOH by Raman spectroscopy compared with XRD is most likely because the Raman signal represents surface species, which is where the initial processes of aging are concentrated.

The effect of aging on the structure of ZVI was characterized by BET gas adsorption and SEM. The BET data (Figure 1C) show that surface area increased monotonically with aging, although there was a sharp increase at 96 h, presumably associated with the depletion of Fe^0 and the appearance of γ-FeOOH. The BET method was also used to characterize the porosity of the ZVI, and these results are reported in Table S1. The images obtained by SEM (Figure S3) show that the pristine ZVI used in this study consisted of relatively smooth spheres, which developed prominent surface defects by 12 h of aging. With prolonging aging time, the ZVI became fully coated with angular-shaped and platy structures that are consistent with magnetite and lepidocrocite.[50] The changes in morphology that can be seen in the SEM are consistent with the increased pore volume measured by BET (Table S1).

Se(IV) Sequestration Kinetics. Figure 2 shows the kinetics of Se(IV) removal for all aging times, with and without WMF. A brief lag phase (10–20 min) can be seen in many of the data obtained with this system, both in this study (Figure 2) and in our previous work.[45,51,52] This feature is relatively less significant in the longer experiments required by the lower overall Se(IV) sequestration rates produced without WMF, with aging, and/or at higher pH. Tailing is evident in the experiments that were run to complete removal of Se(IV), especially those with WMF and intermediate aging, which gave the fastest Se(IV) removal. In our previous work, tailing was also observed under favorable conditions, such as low pH with WMF.[45]

The main portion of each data set, however, can be well described by pseudo-first-order kinetics. The fitting results are shown in Figure 2, and the pseudo-first-order rate constants (k_{obs}) are given in Table S2. The corresponding mass normalized rate constants (k_M) are not given because they have the same values as k_{obs} (ZVI mass concentration was 1 g per L of solution in all experiments). Surface area normalized rate constants (k_{SA}) were then calculated from k_M, and the measured specific surface area (a_s) for each type of ZVI (Table S1) assuming the iron dose-dependence follows the standard kinetic model.[53]

From visual inspection of Figure 2, it is evident that WMF consistently gives faster selenium removal kinetics and that this enhancement is greatest for intermediate aging times. A more detailed view of this trend is provided in Figure S4 by plotting the rate constants for Se(IV) removal (k_{obs} or k_{SA}, from Table S2) vs aging time. The two types of rate constants give similar results, although the trends in k_{SA} are slightly more systematic. The defining features of Figure S4 are 3-fold: (*i*) unaged ZVI (AZVI-0) gives the fastest Se(IV) removal rates, with little increase due to WMF; (*ii*) aging 80 or more hours gives the slowest Se(IV) rates, with little enhancement by WMF; and (*iii*) aging between 6 and 60 h gives nearly constant rates of Se(IV) removal, but with rate constants that are 10- to 100-fold greater with WMF than without. The over 100-fold enhancement—at pH 6.0 using ZVI aged for moderate time periods (24–48 h)—is significantly greater than the maximum enhancement (<50 fold) we observed in previous work where

dx.doi.org/10.1021/es500958b | Environ. Sci. Technol. 2014, 48, 6326–6334

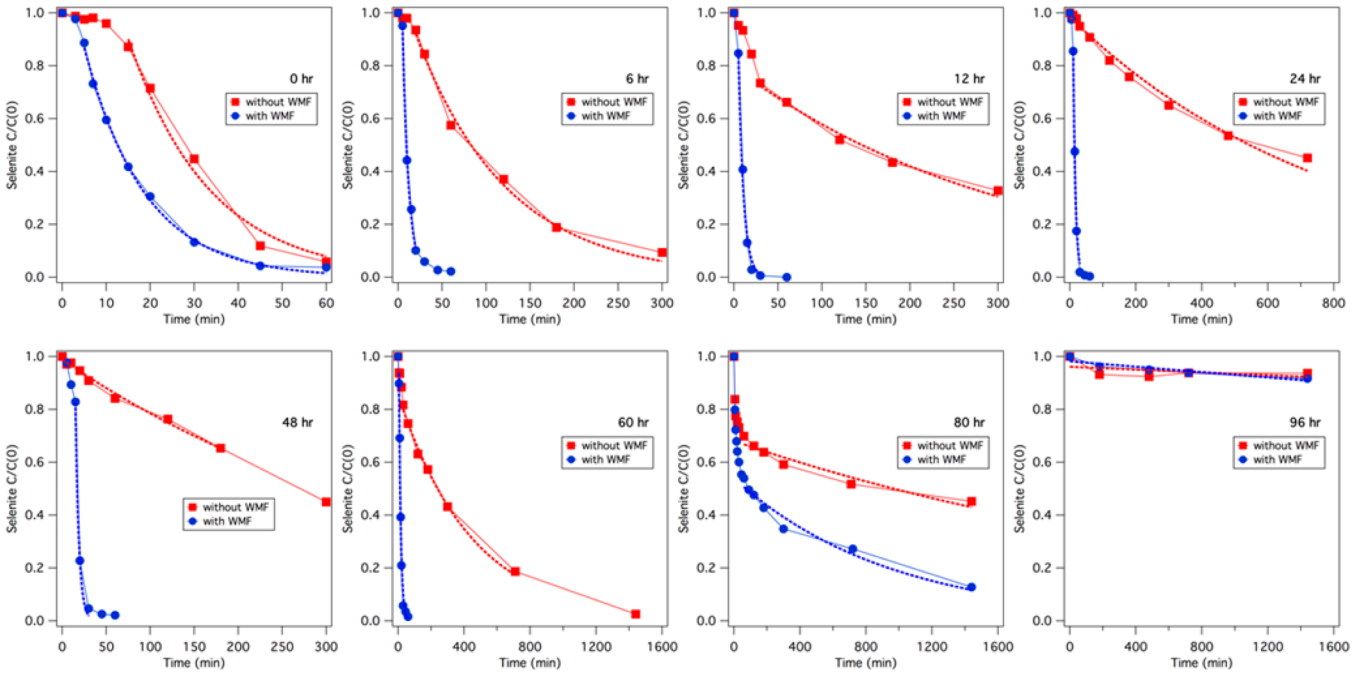

Figure 2. Kinetics of Se(IV) removal by pristine and aged ZVI with and without WMF. All data from stirred, open batch reactors with 1.0 g L^{-1} ZVI, 40.0 mg L^{-1} Se(IV), 0.1 M MES at pH = 6.0. Differences in between replicates were negligible, so only average values are plotted. Dashed lines are fits to first-order kinetics.

we varied initial Se(IV) concentration but did not include aging.[45]

The shapes of the kinetic and aging profiles in Figures 2 and S4, respectively, suggest that the system evolves through three phases. Initially, immersion of the (previously freeze-dried) ZVI initiates processes such as hydration, dissolution, and pitting of the oxide film, which result in increasing corrosion rates (i.e., depassivation) that, in turn, cause increased rates of Se(IV) sequestration. The resulting lag phase in Se(IV) removal is longest for ZVI without prior aging in solution because it has a stable passive film formed by extended exposure to air, whereas the lag phase becomes negligible for ZVI where prior exposure to solution has partially destabilized the passive film. Analogous effects have been seen in previous studies with a variety of ZVIs and contaminants,[54] although no study has investigated these lag phases in detail because they apply to time scales too short to be of practical significance in water treatment applications.

After depassivation of the ZVI, the oxide film appears to have evolved to a relatively consistent and metastable condition that produces uniform rates of Se(IV) sequestration regardless of sample history. This phase produces the largest WMF effect, because the aged oxide film on ZVI is thicker and yet more porous, which makes it more susceptible to magnetic field driven transport effects. This conceptual model for the WMF effect is further elaborated after discussion of material characterization and modeling presented below. Finally, there is little WMF effect on AZVI-80 and none on AZVI-96 because extended aging caused nearly complete conversion of Fe^0 to Fe^{2+}/Fe^{3+} oxides, leaving only the relatively weak adsorption of Se(IV) onto iron oxides as the rate limiting process for Se(IV) sequestration.

Processes Controlling Se(IV) Sequestration. The trends in Se(IV) sequestration kinetics represented in Figure S4 suggest a coupling between aging and WMF effects that is mediated by transformations in the oxide passive film on ZVI. These transformations all involve Fe(II), some of which becomes measurable as Fe^{2+} in solution. Data for dissolved Fe^{2+} vs time is given in Figure S5 for all of the Se(IV) sequestration experiments shown in Figure 2. In general, Fe^{2+} increases with reaction time and is greater with WMF than without, but the trend with aging time appears to be more complex. However, plotting Se(IV) vs Fe^{2+} for each experiment (Figure 3) shows that these two parameters are closely coupled. With a few exceptions (discussed below), the data sets for ZVI with and without WMF fall into two distinct groups: With WMF, sequestration of Se(IV) generally is accompanied by an almost linear increase in Fe^{2+} (Group 1), and without WMF, there is sequestration of Se(IV) but with little increase in Fe^{2+} (Group 2).

The type of analysis represented by Figure 3 (i.e., time series correlations between contaminant removed and dissolved iron released) can be difficult to interpret because there are several processes affecting each variable and coupling between the two is not necessarily direct. However, in this case, the main features of Figure 3 provide insights into the controlling processes in this system that are not clear from the individual time series data (i.e., Figures 2 and S5). The strong correlation between Se(IV) removal and Fe^{2+} release for most experiments with WMF (Group 1) suggests a relatively direct effect: likely reduction of Se(IV) to Se^0 by Fe^0 (i.e., eq 1)

$$2Fe^0 + HSeO_3^- + 5H^+ \rightarrow 2Fe^{2+} + Se^0 \downarrow + 3H_2O \qquad (1)$$

which apparently is sustained by the WMF effect. In contrast, the weak correlation between Se(IV) removal and Fe^{2+} release in experiments without the WMF effect (Group 2) is consistent with adsorption of Se(IV) onto iron oxides being dominant and corrosion of Fe^0 (potentially coupled to reduction of Se(IV)) being slower.

There are a few exceptions to the main groupings in Figure 3, but these provide further support for the overall interpretation.

dx.doi.org/10.1021/es500958b | Environ. Sci. Technol. 2014, 48, 6326−6334

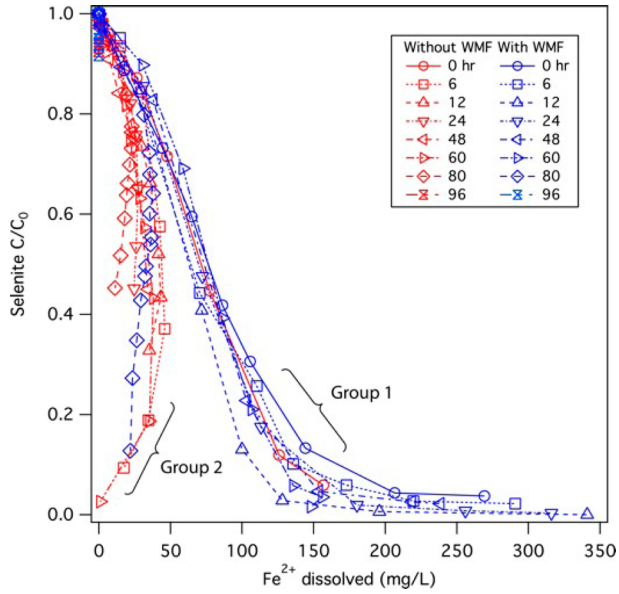

Figure 3. Correlation between Se(IV) and dissolved Fe^{2+} concentrations at each time point of each batch experiment for the 16 combinations of aging time and WMF exposure. The Se(IV) data correspond to those in Figure 2 and the Fe^{2+} are those in Figure S5. Data for 96 h aging are concentrated in the upper-left corner. (Initial conditions: 1.0 g L^{-1} ZVI, 40.0 mg L^{-1} Se(IV), 0.1 M MES at pH = 6.0).

The most conspicuous exception is the tail in the Group 1 data, which results because ZVI continues to corrode (releasing Fe^{2+} according to eq 2) even after all of the Se(IV) is sequestered.

$$2Fe^0 + O_2 + 2H_2O \rightarrow 2Fe^{2+} + 4OH^- \quad (2)$$

The second exception involves the data for AZVI-80 with WMF, which deviates from the other data with WMF and instead follows the trend of data in Group 2. This result, however, is consistent with almost complete oxidation of Fe^0 and the concomitant change in the mechanism of Se(IV) sequestration from reduction (eq 1) to adsorption followed by reduction. The third type of exceptional behavior is by the data for AZVI-96, with and without WMF, which is unresolved in the upper-left corner of Figure 3. In this case, the result arises because Fe^0 was nearly exhausted after 96 h of aging, so there was very little sequestration of Se(IV) or production of Fe^{2+}. The interpretations of the latter two types of exceptions are further supported by the XANES data discussed in the section that follows.

After the lag and before the tail in the Group 1 data, the correlation between Se(IV) removal and Fe^{2+} release is remarkably close for the whole group of experiments (Figure 3). Isolating this portion of the data, as shown in Figure S6, shows that the whole group can be fitted to a single linear relationship, and 1 molar Se(IV) removal approximately corresponds to 5 molar Fe^{2+} release. The robustness of this correlation is strong evidence that eq 1 is the dominant process under these conditions. The amount of Fe^{2+} released from ZVI was much larger than the theoretical value obtained from eq 1, which should be associated with the oxidation of Fe^0 by oxygen since the experiments were performed open to the air.

The defining feature of Group 2 in Figure 3 is the tendency for the Fe^{2+} data to peak and then decline as Se(IV) sequestration approaches completion. The decline in Fe^{2+} as Se(IV) is depleted is most likely due to formation and precipitation of Fe^{3+} by, for example, eq 3.

$$6Fe^{2+} + O_2 + 6H_2O \rightarrow 2Fe_3O_4 \downarrow + 12H^+ \quad (3)$$

Most of the data without WMF follow this pattern, except for AZVI-0, which follows the pattern as most of the experiments with WMF. This result is expected because the unaged ZVI is minimally passivated and therefore behaves similarly with and without WMF (e.g., as in Figure 3).

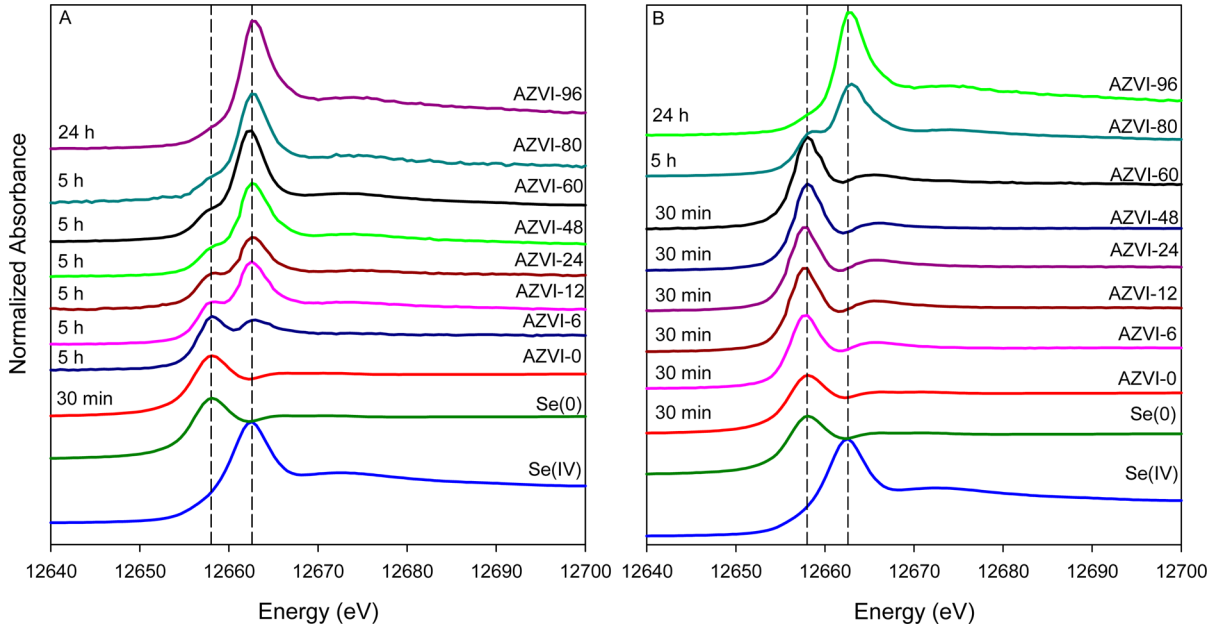

Figure 4. XANES spectra of pristine and aged ZVI particles reacted with 40.0 mg L^{-1} Se(IV) at pH 6.0 open to air in the absence of WMF (A) or in the presence of WMF (B) (1.0 g L^{-1} pristine or AZVI, 40.0 mg L^{-1} Se(IV), pH = 6.0). Se standard materials (selenium powder for Se(0); sodium selenite (Na_2SeO_3) for Se(IV)).

dx.doi.org/10.1021/es500958b | Environ. Sci. Technol. 2014, 48, 6326−6334

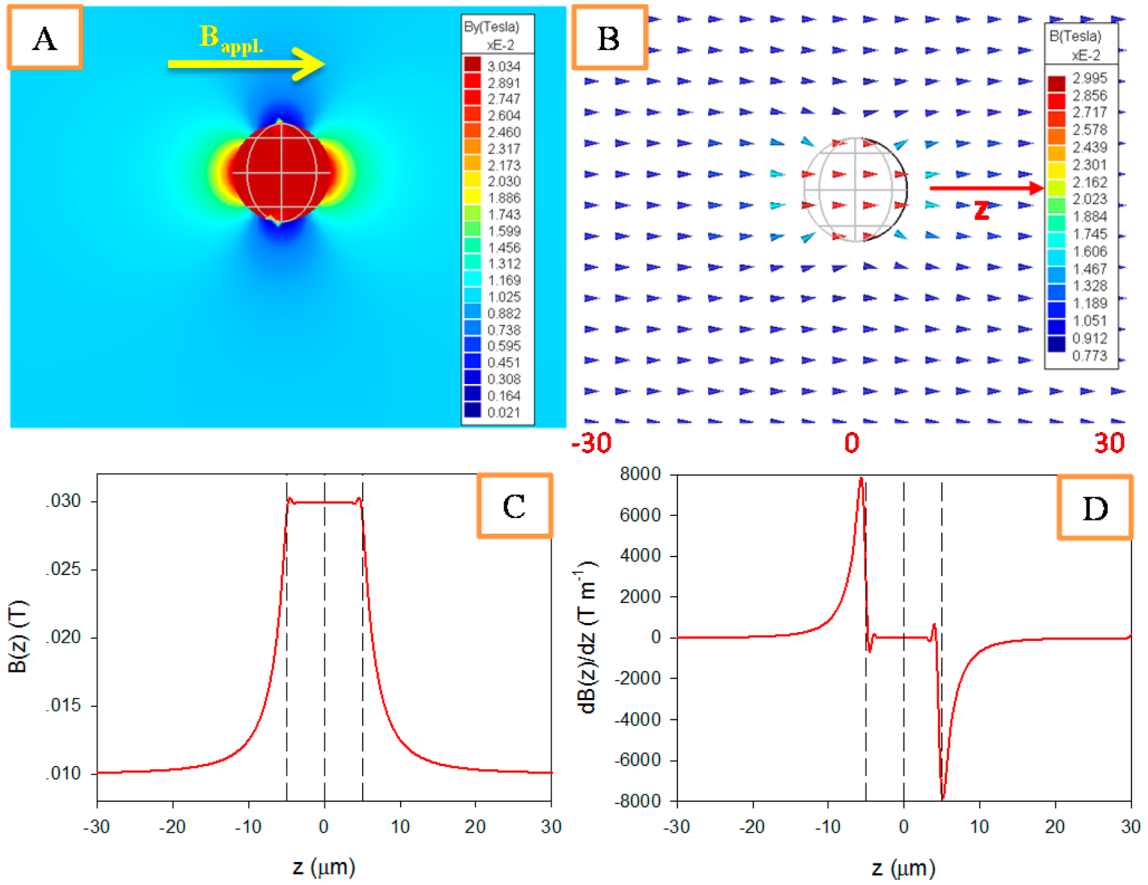

Figure 5. (A) Magnetic field strength distribution of the plane parallel to the applied magnetic field with an applied flux density B_{appl} of 0.01 T and through the center of a ZVI sphere; (B) Vector of the magnetic flux of the plane in (A); (C) The magnetic field strength distribution along the coordinate z, as shown in (B); (D) The magnetic field gradient along the coordinate z.

The interpretations of Figures 2-3 (and S4−S6) are consistent with measurements of DO and ORP (Figures S7−S8), which were made during the same experiments, in a manner similar to what we reported in previous work.[45,51] Unaged ZVI and aged ZVI with WMF are relatively un- or depassivated and therefore react rapidly with DO, whereas aged ZVI without WMF is passivated and does not produce a net decrease in DO. In this system, ORP is expect to reflect both DO and Fe^{2+},[55] so the coupled effects of aging and WMF should be reflected in ORP. This is supported by qualitative comparison of Figure S8 with Figures S5 and S7.

Material Characterization of Sequestered Se(IV). To explore the speciation of Se(IV) that was sequestered on ZVI over the range of conditions used in this study, Se *K*-edge XANES spectra were obtained on solids recovered after exposure times corresponding roughly to the end of the experiments shown in Figure 2. The results are shown in Figure 4, together with data for Se(0) and Se(IV) reference materials, which have *K*-edge energies (E_0) at 12,658.0 eV and 12,662.6, respectively.

The XANES spectra of Se(VI)-treated ZVI in Figure 4 clearly show that there is reduction of Se(IV) to Se(0), consistent with our previous studies.[45,52] However, without WMF (Figure 4A), the degree of reduction to Se(0) decreased with aging of the ZVI, despite substantial removal of Se(IV) from solution (c.f., Figure 2), suggesting a shift in sequestration mechanism from reduction to adsorption followed by reduction to adsorption only. With WMF (Figure 4B), the effect of aging on the Se(IV) sequestration mechanism was less, so the process was dominated by reduction to Se(0) until aging time exceeded 60 h. With 80 h of aging, only a small fraction of the Se(IV) sequestrated was reduced to Se(0) in 5 h of reaction time in the presence of WMF, which is consistent with depletion of Fe^0 in AZVI-80. After 96 h of aging, negligible reduction of Se(IV) to Se(0) was observed over 24 h with and without WMF, due to the nearly complete exhaustion of Fe^0. These changes in Se(IV) sequestration mechanism due to the coupled effects of aging and WMF are summarized graphically in Figure S9.

Characterization of the Magnetic Field and Resulting Forces. Due to the ferromagnetic nature of ZVI, it becomes magnetized upon exposure to a magnetic field. This magnetization leads to a strongly inhomogeneous field over the iron surface, with a flux density that can exceed that of the external field. These conditions lead to two types of magnetic forces that can affect a reaction that is carried out in an external magnetic field.[56] One, known as the Lorentz force (F_L, N m^{-3}), arises from the magnetic field acting on charged species and is described by the Lorentz equation (eq 4). The other, known as the magnetic gradient force ($F_{\Delta B}$, N m^{-3}), is induced by a magnetic field at an interface as it acts on paramagnetic ions in the boundary layer and is described by eq 5[57,58]

$$F_L = J \times B \tag{4}$$

$$F_{\Delta B} = (\chi/\mu_0)B(z)\frac{dB(z)}{dz} \tag{5}$$

dx.doi.org/10.1021/es500958b | Environ. Sci. Technol. 2014, 48, 6326−6334

where J is the flux of charged species (coulombs cm^{-2} s^{-1}), B is the external magnetic field (Tesla), χ is the molar magnetic susceptibility (m^3 mol^{-1}), μ_0 is the magnetic permeability of vacuum (equal to $4 \times \pi \times 10^{-7}$ N A^{-2}), and $B(z)$ is the magnetic field strength at position z (distance on the axis perpendicular to the surface).[56,57]

To evaluate the flux density distribution near the ZVI sphere surface, numerical simulations were performed, assuming a 10 μm diameter spherical particle of pure ZVI in an externally applied magnetic field with homogeneous flux density (B_{appl}) equal to 10 mT (similar to what was provided by the magnet used in the Se(IV) sequestration experiments described above). The results are shown in Figure 5.

The intensity and direction of the magnetic field associated with a sphere of ZVI while exposed to a homogeneous magnetic field are shown in Figures 5 A and B, respectively. Concentrations of magnetic flux density can be seen at the particle surface near the magnetic poles, which are aligned to the z axis. The distribution of magnetic flux density along the z axis is shown in Figure 5(C). B_z increases sharply from the background value provided by the external magnet (10.3 mT at $z = -19.8$ μm) to a maximum at the ZVI/medium interface (30 mT at $z = -4.8$ μm). The corresponding magnetic field gradient (dB_z/dz), which is shown in Figure 5(D), has a maximum value of 7154 T m^{-1} at $z = -6.0$ μm, which is 1.0 μm away from the ZVI surface.

At the point of peak field gradient ($z = -4.8$ μm), the calculated magnetic forces acting on Fe^{2+} are F_L = 0.17 N m^{-3} and $F_{\Delta B}$ = 64.4 N m^{-3} (the molar magnetic susceptibility is 14750×10^{-9} L mol^{-1}[59] and assuming the Fe^{2+} concentration is 0.01 M). The Lorentz force can give rise to convection in the solution which narrows the diffusion layer and enhances mass transportation.[60] The field gradient force tends to move paramagnetic ions (Fe^{2+}) along the higher field gradient at the ZVI particle surface, which creates localized galvanic couples and electromagnetic forces that stimulate migration of ions, breakdown of the passive film, and eventually localized corrosion.[45,61] Direct evidence for the resulting inhomogeneous distribution of Fe^{2+} can be seen in Figure S10, and direct evidence for localized corrosion is provided in Figure S11.

PRACTICAL IMPLICATIONS

Prior to this and our other recent work,[45] there appears to be only one published study that directly addressed the effect of a magnetic field on contaminant removal by (unaged) ZVI.[62] A few other studies make prominent use of magnetic fields to control bulk particle transport and mixing,[63,64] but their methods were not designed to test for magnetic field effects on ZVI reactivity and no effects were noted. It is possible that many studies of ZVI reactivity have been done using magnetic stirring devices, but this methodological detail is not usually documented in a way that can be used as a literature search criteria, so it is difficult to systematically identify prior work that might exhibit WMF effects that were not recognized at the time. One practical implication of the results of this study, however, should be that the possibility of WMF effects becomes a more carefully controlled experimental variable in future studies.

The broader implications of this work (showing potentially beneficial WMF effects) on field-scale remediation practices are intriguing but require further investigation. Although generating a WMF around a large scale ZVI-based filter or permeable reactive barrier (PRB) is costly, pretreatment to magnetize ZVI prior to field deployment is technically feasible, and the practicality and long-term benefits remain to be demonstrated. The results of this work suggest that magnetization after deployment might provide a noninvasive way to maintain or restore the reactivity of ZVI even after there has been substantial accumulation of passivating oxides. This method might be most applicable to PRBs emplaced in aerobic aquifers and in above-ground canisters or filter beds, where passivation by accumulation of iron oxides is most severe.[65,66] A wide range of mineral precipitates including Fe_3O_4 and γ-FeOOH has been identified in ZVI-based household filters and in PRBs, depending on the degree of iron oxidation, groundwater chemistry and microbial activity.[66,67] Therefore, ZVI samples aged under different conditions are being synthesized in our lab, and the feasibility of employing WMF to restore the reactivity of aged ZVI passivated by various corrosion products is to be explored.

ASSOCIATED CONTENT

Supporting Information

Two texts, 11 figures, and two tables. This material is available free of charge via the Internet at http://pubs.acs.org.

AUTHOR INFORMATION

Corresponding Authors

*Phone: +86-451-86283010. E-mail: hitgxh@126.com (X.G.).
*Phone: 503-346-3431. E-mail: tratnyek@ohsu.edu (P.G.T.).

Notes

The authors declare no competing financial interest.

ACKNOWLEDGMENTS

This work was supported by the National Natural Science Foundation of China (21277095), the Specialized Research Fund for the Doctoral Program of Higher Education (20130072110026), and the 111 Project. The authors thank beamline BL14W1 (Shanghai Synchrotron Radiation Facility) for providing the beam time (z13sr0023) and Dr. Xiaolei Zhang for his help in performing the numerical simulation. Funding for contributions of PGT came from the U.S. National Science Foundation, Environmental Engineering Program (CBET-1333476).

REFERENCES

(1) Khudenko, B. M. Mechanism and kinetics of cementation processes. *Water. Sci. Technol.* **1985**, *17*, 719−732.
(2) Li, X. Q.; Zhang, W. X. Sequestration of metal cations with zerovalent iron nanoparticles - A study with high resolution x-ray photoelectron spectroscopy (HR-XPS). *J. Phys. Chem. C* **2007**, *111*, 6939−6946.
(3) Yan, W.; Ramos, M. A. V.; Koel, B. E.; Zhang, W. X. As(III) sequestration by iron nanoparticles: Study of solid-phase redox transformations with X-ray photoelectron spectroscopy. *J. Phys. Chem. C* **2012**, *116*, 5303−5311.
(4) Blowes, D. W.; Ptacek, C. J.; Benner, S. G.; McRae, C. W. T.; Bennett, T. A.; Puls, R. W. Treatment of inorganic contaminants using permeable reactive barriers. *J. Contam. Hydrol.* **2000**, *45*, 123−137.
(5) Naftz, D. L.; Morrison, S. J.; Davis, J. A.; Fuller, C. C., Eds. *Handbook of Groundwater Remediation using Permeable Reactive Barriers: Applications to Radionuclides, Trace Metals, and Nutrients*; Academic Press: San Diego, CA, 2002.
(6) Gould, J. P. The kinetics of hexavalent chromium reduction by metallic iron. *Water Res.* **1982**, *16*, 871−877.

(7) Melitas, N.; Farrell, J. Understanding chromate reaction kinetics with corroding iron media using Tafel analysis and electrochemical impedance spectroscopy. *Environ. Sci. Technol.* **2002**, *36*, 5476−5482.
(8) Wilkin, R. T.; Su, C. M.; Ford, R. G.; Paul, C. J. Chromium-removal processes during groundwater remediation by a zerovalent iron permeable reactive barrier. *Environ. Sci. Technol.* **2005**, *39*, 4599−4605.
(9) Su, C.; Puls, R. W. In situ remediation of arsenic in simulated groundwater using zerovalent iron: Laboratory column tests on combined effects of phosphate and silicate. *Environ. Sci. Technol.* **2003**, *37*, 2582−2587.
(10) Lackovic, J. A.; Nikolaidis, N. P.; Dobbs, G. M. Inorganic arsenic removal by zero-valent iron. *Environ. Eng. Sci.* **2000**, *17*, 29−39.
(11) Wilkin, R. T.; Acree, S. D.; Ross, R. R.; Beak, D. G.; Lee, T. R. Performance of a zerovalent iron reactive barrier for the treatment of arsenic in groundwater: Part 1. Hydrogeochemical studies. *J. Contam. Hydrol.* **2009**, *106*, 1−14.
(12) Gu, B.; Liang, L.; Dickey, M. J.; Yin, X.; Dai, S. Reductive precipitation of uranium(VI) by zero-valent iron. *Environ. Sci. Technol.* **1998**, *32*, 3366−3373.
(13) Farrell, J.; Bostick, W. D.; Jarabek, R. J.; Fiedor, J. N. Uranium removal from ground water using zero valent iron media. *Ground Water* **1999**, *37*, 618−624.
(14) Noubactep, C.; Schoner, A.; Meinrath, G. Mechanism of uranium removal from the aqueous solution by elemental iron. *J. Hazard. Mater.* **2006**, *132*, 202−212.
(15) Noubactep, C. An analysis of the evolution of reactive species in Fe^0/H_2O systems. *J. Hazard. Mater.* **2009**, *168*, 1626−1631.
(16) Xie, Y.; Cwiertny, D. M. Use of dithionite to extend the reactive lifetime of nanoscale zero-valent iron treatment systems. *Environ. Sci. Technol.* **2010**, *44*, 8649−8655.
(17) Turcio-Ortega, D.; Fan, D.; Tratnyek, P. G.; Kim, E. J.; Chang, Y. S. Reactivity of Fe/FeS nanoparticles: Electrolyte composition effects on corrosion electrochemistry. *Environ. Sci. Technol.* **2012**, *46*, 12484−12492.
(18) Mylon, S. E.; Sun, Q.; Waite, T. D. Process optimization in use of zero valent iron nanoparticles for oxidative transformations. *Chemosphere* **2010**, *81*, 127−131.
(19) Schlicker, O.; Ebert, M.; Fruth, M.; Weidner, M.; Wüst, W. F.; Dahmke, A. Degradation of TCE with iron: The role of competing chromate and nitrate reduction. *Ground Water* **2000**, *38*, 403−409.
(20) Su, C.; Puls, R. W. Arsenate and arsenite removal by zerovalent iron: Effects of phosphate, silicate, carbonate, borate, sulfate, molybdate, and nitrate, relative to chloride. *Environ. Sci. Technol.* **2001**, *35*, 4562−4568.
(21) Ritter, K.; Odziemkowski, M. S.; Simpgraga, R.; Gillham, R. W.; Irish, D. E. An in situ study of the effect of nitrate on the reduction of trichloroethylene by granular iron. *J. Contam. Hydrol.* **2003**, *65*, 121−136.
(22) Agrawal, A.; Ferguson, W. J.; Gardner, B. O.; Christ, J. A.; Bandstra, J. Z.; Tratnyek, P. G. Effects of carbonate species on the kinetics of dechlorination of 1,1,1-trichloroethane by zero-valent iron. *Environ. Sci. Technol.* **2002**, *36*, 4326−4333.
(23) Jeen, S. W.; Gillham, R. W.; Blowes, D. W. Effects of carbonate precipitates on long-term performance of granular iron for reductive dechlorination of TCE. *Environ. Sci. Technol.* **2006**, *40*, 6432−6437.
(24) Lo, I. M. C.; Lam, C. S. C.; Lai, K. C. K. Hardness and carbonate effects on the reactivity of zero-valent iron for Cr(VI) removal. *Water Res.* **2006**, *40*, 595−605.
(25) Kim, E. J.; Murugesan, K.; Kim, J. H.; Tratnyek, P. G.; Chang, Y. S. Remediation of trichloroethylene by FeS-coated iron nanoparticles in simulated and real groundwater: Effects of water chemistry. *Ind. Eng. Chem. Res.* **2013**, *52*, 9343−9350.
(26) Liu, T. X.; Li, X.; Waite, T. D. Depassivation of aged Fe^0 by ferrous ions: Implications to contaminant degradation. *Environ. Sci. Technol.* **2013**, *47*, 13712−13720.
(27) Liu, T. X.; Li, X.; Waite, T. D. Depassivation of aged Fe^0 by inorganic salts: Implications to contaminant degradation in seawater. *Environ. Sci. Technol.* **2013**, *47*, 7350−7356.
(28) Zhang, M.; He, F.; Zhao, D.; Hao, X. Degradation of soil-sorbed trichloroethylene by stabilized zero valent iron nanoparticles: Effects of sorption, surfactants, and natural organic matter. *Water Res.* **2011**, *45*, 2401−2414.
(29) Park, H.; Kanel Sushil, R.; Choi, H. Arsenic removal by nano-scale zero valent iron and how it is affected by natural organic matter. In *Environmental Applications of Nanoscale and Microscale Reactive Metal Particles*; Geiger, C. L., Carvalho-Knighton, K. M., Eds.; American Chemical Society: Washington, DC, 2009; ACS Symposium Series, Vol. *1027*, pp 135−161.
(30) Phenrat, T.; Liu, Y.; Tilton, R. D.; Lowry, G. V. Adsorbed polyelectrolyte coatings decrease Fe^0 nanoparticle reactivity with TCE in water: Conceptual model and mechanisms. *Environ. Sci. Technol.* **2009**, *43*, 1507−1514.
(31) Reinsch, B. C.; Forsberg, B.; Penn, R. L.; Kim, C. S.; Lowry, G. V. Chemical transformations during aging of zerovalent iron nanoparticles in the presence of common groundwater dissolved constituents. *Environ. Sci. Technol.* **2010**, *44*, 3455−3461.
(32) Wang, Q.; Lee, S.; Choi, H. Aging study on the structure of Fe^0-nanoparticles: Stabilization, characterization, and reactivity. *J. Phys. Chem. C* **2010**, *114*, 2027−2033.
(33) Yan, W.; Herzing, A. A.; Li, X. Q.; Kiely, C. J.; Zhang, W. X. Structural evolution of Pd-doped nanoscale zero-valent iron (nZVI) in aqueous media and implications for particle aging and reactivity. *Environ. Sci. Technol.* **2010**, *44*, 4288−4294.
(34) Sarathy, V.; Tratnyek, P. G.; Nurmi, J. T.; Baer, D. R.; Amonette, J. E.; Chun, C.; Penn, R. L.; Reardon, E. J. Aging of iron nanoparticles in aqueous solution: Effects on structure and reactivity. *J. Phys. Chem. C* **2008**, *112*, 2286−2293.
(35) Matheson, L. J.; Tratnyek, P. G. Reductive dehalogenation of chlorinated methanes by iron metal. *Environ. Sci. Technol.* **1994**, *28*, 2045−2053.
(36) Agrawal, A.; Tratnyek, P. G. Reduction of nitro aromatic compounds by zero-valent iron metal. *Environ. Sci. Technol.* **1996**, *30*, 153−160.
(37) Lai, K. C. K.; Lo, I. M. C. Removal of chromium (VI) by acid-washed zero-valent iron under various groundwater geochemistry conditions. *Environ. Sci. Technol.* **2008**, *42*, 1238−1244.
(38) Lin, C. J.; Lo, S. L. Effects of iron surface pretreatment on sorption and reduction kinetics of trichloroethylene in a closed batch system. *Water Res.* **2005**, *39*, 1037−1046.
(39) Geiger, C. L.; Ruiz, N. E.; Clausen, C. A.; Reinhart, D. R.; Quinn, J. W. Ultrasound pretreatment of elemental iron: Kinetic studies of dehalogenation reaction enhancement and surface effects. *Water Res.* **2002**, *36*, 1342−1350.
(40) Hung, H. M.; Hoffmann, M. R. Kinetics and mechanism of the enhanced reductive degradation of CCl_4 by elemental iron in the presence of ultrasound. *Environ. Sci. Technol.* **1998**, *32*, 3011−3016.
(41) Liu, H.; Li, G.; Qu, J.; Liu, H. Degradation of azo dye Acid Orange 7 in water by Fe^0/granular activated carbon system in the presence of ultrasound. *J. Hazard. Mater.* **2007**, *144*, 180−186.
(42) Ziylan, A.; Koltypin, Y.; Gedanken, A.; Ince, N. H. More on sonolytic and sonocatalytic decomposition of Diclofenac using zero-valent iron. *Ultrason. Sonochem.* **2013**, *20*, 580−586.
(43) Lu, X.; Li, M.; Tang, C.; Feng, C.; Liu, X. Electrochemical depassivation for recovering Fe^0 reactivity by Cr(VI) removal with a permeable reactive barrier system. *J. Hazard. Mater.* **2012**, *213-214*, 355−360.
(44) Chen, L.; Jin, S.; Fallgren, P. H.; Swoboda-Colberg, N. G.; Liu, F.; Colberg, P. J. S. Electrochemical depassivation of zero-valent iron for trichloroethene reduction. *J. Hazard. Mater.* **2012**, *239−240*, 265−269.
(45) Liang, L. P.; Sun, W.; Guan, X. H.; Huang, Y. Y.; Choi, W.; Bao, H. L.; Li, L. N.; Jiang, Z. Weak magnetic field significantly enhances selenite removal kinetics by zero valent iron. *Water Res.* **2014**, *49*, 371−380.
(46) Stookey, L. L. Ferrozine-A new spectrophotometric reagent for iron. *Anal. Chem.* **1970**, *42*, 779−781.

(47) Liu, Y.; Lowry, G. V. Effect of particle age (Fe^0 content) and solution pH on nZVI reactivity: H_2 evolution and TCE dechlorination. *Environ. Sci. Technol.* **2006**, *40*, 6085−6090.
(48) Slavov, L.; Abrashev, M. V.; Merodiiska, T.; Gelev, C.; Vandenberghe, R. E.; Markova-Deneva, I.; Nedkov, I. Raman spectroscopy investigation of magnetite nanoparticles in ferrofluids. *J. Magn. Magn. Mater.* **2010**, *322*, 1904−1911.
(49) de Faria, D. L. A.; Venâncio Silva, S.; de Oliveira, M. T. Raman microspectroscopy of some iron oxides and oxyhydroxides. *J. Raman Spectrosc.* **1997**, *28*, 873−878.
(50) Cornell, R. M.; Schwertmann, U. *The Iron Oxides: Structure, Properties, Reactions, Occurences and Uses*; Wiley-VCH Verlag GmbH & Co. KGaA: Weinheim, Germany, 2003.
(51) Liang, L. P.; Jiang, X.; Yang, W. J.; Huang, Y. Y.; Guan, X. H.; Li, L. N. Kinetics of selenite reduction by zero-valent iron. *Desalin. Water Treat.* **2013**, DOI: 10.1080/19443994.2013.862868.
(52) Liang, L. P.; Yang, W. J.; Guan, X. H.; Li, J. L.; Xu, Z. J.; Wu, J.; Huang, Y. Y.; Zhang, X. Z. Kinetics and mechanisms of pH-dependent selenite removal by zero valent iron. *Water Res.* **2013**, *47*, 5846−5855.
(53) Johnson, T. L.; Scherer, M. M.; Tratnyek, P. G. Kinetics of halogenated organic compound degradation by iron metal. *Environ. Sci. Technol.* **1996**, *30*, 2634−2640.
(54) Miehr, R.; Tratnyek, P. G.; Bandstra, J. Z.; Scherer, M. M.; Alowitz, M.; Bylaska, E. J. The diversity of contaminant reduction reactions by zero-valent iron: role of the reductate. *Environ. Sci. Technol.* **2004**, *38*, 139−147.
(55) Shi, Z.; Nurmi, J. T.; Tratnyek, P. G. Effects of nano zero-valent iron (nZVI) on oxidation-reduction potential (ORP). *Environ. Sci. Technol.* **2011**, *45*, 1586−1592.
(56) Ragsdale, S. R.; Grant, K. M.; White, H. S. Electrochemically generated magnetic forces. Enhanced transport of a paramagnetic redox species in large, nonuniform magnetic fields. *J. Am. Chem. Soc.* **1998**, *120*, 13461−13468.
(57) Tanimoto, Y.; Katsuki, A.; Yano, H.; Watanabe, S.-i. Effect of high magnetic field on the silver deposition from its aqueous solution. *J. Phys. Chem. A* **1997**, *101*, 7359−7363.
(58) Fujiwara, M.; Mitsuda, K.; Tanimoto, Y. Movement and diffusion of paramagnetic ions in a magnetic field. *J. Phys. Chem. B* **2006**, *110*, 13965−13969.
(59) Phipps, J.; Huffman, D. Magnetic susceptibility of the elements and inorganic compounds. 2000. http://www-d0.fnal.gov/hardware/cal/lvps_info/engineering/elementmagn.pdf (accessed 2/2014).
(60) Lioubashevski, O.; Katz, E.; Willner, I. Magnetic field effects on electrochemical processes: A theoretical hydrodynamic model. *J. Phys. Chem. B* **2004**, *108*, 5778−5784.
(61) Sueptitz, R.; Tschulik, K.; Uhlemann, M.; Schultz, L.; Gebert, A. Effect of high gradient magnetic fields on the anodic behaviour and localized corrosion of iron in sulphuric acid solutions. *Corros. Sci.* **2011**, *53*, 3222−3230.
(62) Kim, D. H.; Kim, J.; Choi, W. Effect of magnetic field on the zero valent iron induced oxidation reaction. *J. Hazard. Mater.* **2011**, *192*, 928−931.
(63) Graham, L. J.; Jovanovic, G. Dechlorination of p-chlorophenol on a Pd/Fe catalyst in a magnetically stabilized fluidized bed; Implications for sludge and liquid remediation. *Chem. Eng. Sci.* **1999**, *54*, 3085−3093.
(64) Devlin, J. F.; Allin, K. O. Major anion effects on the kinetics and reactivity of granular iron in glass-encased magnet batch reactor experiments. *Environ. Sci. Technol.* **2005**, *39*, 1868−1874.
(65) Mackenzie, P. D.; Horney, D. P.; Sivavec, T. M. Mineral precipitation and porosity losses in granular iron columns. *J. Hazard. Mater.* **1999**, *68*, 1−17.
(66) Neumann, A.; Kaegi, R.; Voegelin, A.; Hussam, A.; Munir, A. K. M.; Hug, S. J. Arsenic removal with composite iron matrix filters in Bangladesh: A field and laboratory study. *Environ. Sci. Technol.* **2013**, *47*, 4544−4554.
(67) Roh, Y.; Lee, S. Y.; Elless, M. P. Characterization of corrosion products in the permeable reactive barriers. *Environ. Geol.* **2000**, *40*, 184−194.